Biosensors and Bioelectronics 49 (2013) 1–8

Contents lists available at SciVerse ScienceDirect

Biosensors and Bioelectronics

journal homepage: www.elsevier.com/locate/bios

Fe_3O_4 magnetic nanoparticles/reduced graphene oxide nanosheets as a novel electrochemical and bioeletrochemical sensing platform

Hazhir Teymourian [a], Abdollah Salimi [a,b,*], Somayeh Khezrian [a]

[a] Department of Chemistry, University of Kurdistan, 66177-15175, Sanandaj, Iran
[b] Research Center for Nanotechnology, University of Kurdistan, 66177-15175, Sanandaj, Iran

ARTICLE INFO

Article history:
Received 12 March 2013
Received in revised form
5 April 2013
Accepted 15 April 2013
Available online 30 April 2013

Keywords:
Fe_3O_4 nanoparticles
Reduced graphene
H_2O_2
NADH
Lactate biosensor
Simultaneous determination

ABSTRACT

We have developed Fe_3O_4 magnetic nanoparticles/reduced graphene oxide nanosheets modified glassy carbon (Fe_3O_4/r-GO/GC) electrode as a novel system for the preparation of electrochemical sensing platform. Decorating Fe_3O_4 nanoparticles on graphene sheets was performed via a facile one-step chemical reaction strategy, where the reduction of GO and the in-situ generation of Fe_3O_4 nanoparticles occurred simultaneously. Characterization of as-made nanocomposite using X-ray diffraction (XRD), transmission electron microscopy (TEM) and alternative gradient force magnetometry (AGFM) clearly demonstrate the successful attachment of monodisperse Fe_3O_4 nanoparticles to graphene sheets. Electrochemical studies revealed that the Fe_3O_4/r-GO/GC electrode possess excellent electrocatalytic activities toward the low potential oxidation of NADH (0.05 V vs. Ag/AgCl) as well as the catalytic reduction of O_2 and H_2O_2 at reduced overpotentials. Via immobilization of lactate dehydrogenase (LDH) as a model dehydrogenase enzyme onto the Fe_3O_4/r-GO/GC electrode surface, the ability of modified electrode for biosensing lactate was demonstrated. In addition, using differential pulse voltammetry (DPV) to investigate the electrochemical oxidation behavior of ascorbic acid (AA), dopamine (DA) and uric acid (UA) at Fe_3O_4/r-GO/GC electrode, the high electrocatalytic activity of the modified electrode toward simultaneous detection of these compounds was indicated. Finally, based on the strong electrocatalytic action of Fe_3O_4/r-GO/GC electrode toward both oxidation and reduction of nitrite, a sensitive amperometric sensor for nitrite determination was proposed. The Fe_3O_4/r-GO hybrid presented here showing favorable electrochemical features may hold great promise to the development of electrochemical sensors, molecular bioelectronic devices, biosensors and biofuel cells.

1. Introduction

Graphene has been the major focus of recent research to exploit an sp^2 hybrid carbon network in applications such as capacitors, cell images, sensors, devices, drug delivery, and solar cell (Wang et al., 2008) due to its unique electronic, mechanical and thermal properties (Li et al., 2008). In addition, graphene is an ideal material for electrochemistry (Pumera, 2009; Navaee et al., 2012; Zhou et al., 2009) because of its very large 2-D electrical conductivity (550 S cm^{-1}), large surface area (2630 m^2 g^{-1}) and a large number of electrochemically favorable edge carbons per mass of graphene which facilitate electron transfer between molecules to an electrode substrate with a low overpotential.

Besides the applications of graphene oxide (GO) and reduced graphene oxide (r-GO), integration of nanoparticles (NPs) and graphene into nanocomposites has recently become a hot topic of research due to their new and/or enhanced functionalities that cannot be achieved by either component alone, and therefore holds great promise for a wide variety of applications in catalysis, optoeletronic materials, surface enhanced Raman Scattering, biomedical fields, and so on (Si and Samulski, 2008; Cong et al., 2010; He et al., 2010). Among them are nanocomposites of magnetic NPs (MNPs), especially iron oxide (either Fe_3O_4 or Fe_2O_3), and graphene oxide (GO) (Fe_3O_4/GO), for potential applications in enhanced optical limiting, MRI, drug delivery, energy storage and removal of contaminants from wastewater (Cong et al., 2010; He et al., 2010; He and Gao, 2010; Chandra et al., 2010; Su et al., 2011). Thus far, although a number of researchers have proposed methods for the preparation of magnetic graphene finding applications in various fields, only a few of them have managed to apply these hybrids for electrochemical sensing or biosensing purposes (Tang et al., 2011; He et al., 2011; Ye et al., 2012).

Herein, via applying different kinds of important compounds as representative examples, the usefulness of the magnetic graphene hybrid for sensing and biosensing purposes will be

* Correspondence to: University of Kurdistan, Department of Chemistry, Pasdaran Street, 66177-15175, Sanandaj, Iran. Tel.: +98 871 662 4001; fax: +98 871 662 4008.
E-mail addresses: absalimi@yahoo.com, absalimi@uok.ac.ir (A. Salimi).

0956-5663/$ - see front matter © 2013 Elsevier B.V. All rights reserved.
http://dx.doi.org/10.1016/j.bios.2013.04.034

strictly demonstrated. At first, the Fe_3O_4/r-GO nanocomposite was synthesized through a simple approach in which the reduction of GO to graphene and the in situ formation of Fe_3O_4 NPs on graphene sheets are accomplished in a one-step reaction. The as-prepared nanocomposite possesses both the electrically conductive and superparamagnetic properties as well as a good dispersibility in polar solvents. After the nanocomposite has been well characterized and the stable formation of Fe_3O_4 NPs on graphene has been confirmed, the potential applicability of the nanocomposite modified GC electrode as an electrochemical sensing platform has been investigated. The electrocatalytic behaviors of different kinds of important electroactive compounds at the Fe_3O_4/r-GO/GC electrode were assessed. In summary, a better electrochemical performance and higher electrocatalytic behavior towards reduction of O_2 and H_2O_2 was obtained at the Fe_3O_4/r-GO/GC electrode compared with r-GO/GC or Fe_3O_4/GC electrodes. In addition, the electrochemical experiments revealed the great ability of Fe_3O_4/r-GO/GC electrode to catalyze ß-nicotinamide adenine dinucleotide (NADH) electrooxidation at a very low potential (0.05 V vs. Ag/AgCl) after which with the successful confinement of L-lactate dehydrogenase (LDH) as a model NAD^+-dependent dehydrogenase enzyme, an effective lactate biosensor was developed. The electrochemical oxidation behaviors of AA, DA and UA at the Fe_3O_4/r-GO/GC electrode were also investigated. Finally, relying on the strong electrocatalytic action of Fe_3O_4/r-GO/GC electrode toward both oxidation and reduction of nitrite, a sensitive amperometric sensor for nitrite determination has been reported.

2. Experimental

The details of experiments are given in Supporting Information (SI). In brief, GO was synthesized by using the modified Hummers method (Hummers and Offeman, 1958) through oxidation of graphite powder. The Fe_3O_4/r-GO nanocomposite was synthesized according to a previously described procedure with a slight modification (Chandra et al., 2010) using ammonia solution (30%) and hydrazine hydrate at a temperature of 90 °C and pH=10. Reduced graphene oxide nanosheets (r-GO) for control experiments were obtained by reduction of GO with hydrazine as described previously (Wang et al., 2009). Fe_3O_4 nanoparticles for AGFM and control electrochemical experiments were prepared using Massart's method (Massart, 1981).

3. Results and discussion

3.1. Characterization of Fe_3O_4/r-GO

TEM was used to reveal the internal structure of the nanocomposite. The low- and high- magnification TEM images of e_3O_4/r-GO hybrid are shown in Fig. 1 A and B. It is evident that two-dimensional r-GO sheets are well decorated by a large quantity of spherical Fe_3O_4 nanostructures (with average size of ~20 nm and rather good size distribution) and both the outline of r-GO and Fe_3O_4 nanoparticles can be clearly observed. The Fe_3O_4 nanoparticles are not simply mixed up or blended with r-GO; rather, they are entrapped inside the r-GO sheets.

Fig. 1C shows the X-ray diffraction (XRD) patterns of the Fe_3O_4/r-GO nanocomposite. As can be seen, the pattern of Fe_3O_4/r-GO displayed obvious diffraction peaks of Fe_3O_4, and the peak positions and relative intensities match well with the standard XRD data for magnetite (JCPDS card, file No. 75-0033). The very weak and broad peak around 23.9° corresponds to r-GO (Zhu et al., 2010) and derived from the short range order in stacked graphene sheets, indicating the reduction of GO during reaction process.

The magnetic properties of Fe_3O_4 nanoparticles and Fe_3O_4/r-GO nanocomposite were examined with AGFM. Fig. 1 D gives the room temperature magnetization hysteresis loops with an applied magnetic field sweeping from −5 to +5kOe. For both profiles of the magnetization curves of Fe_3O_4 and Fe_3O_4/r-GO, the magnetic remanences are nearly zero. This result indicates that there is almost no remaining magnetization when the external magnetic field is removed which is characteristic of superparamagnetic behavior. The Fe_3O_4/r-GO nanocomposite showed a decrease in saturation magnetization compared to the Fe_3O_4 nanoparticles that is explained by decrease in the amount of magnetic component in the nanocomposite. Our results are in good agreement with the results previously reported by other groups (Chandra et al., 2010; Su et al., 2011).

3.2. Electrochemical behavior of Fe_3O_4/r-GO/GC

The effective surface area (A) for different electrodes of GC, Fe_3O_4/GC, r-GO/GC and Fe_3O_4/r-GO/GC was determined from cyclic voltammograms of 0.1 mM $K_4[Fe(CN)_6]$ in PBS (pH 7). The values of A for different electrodes were determined as Fe_3O_4/r-GO/GC (0.0442 cm^{-2}) > r-GO/GC (0.0428 cm^{-2}) > GC (0.0314 cm^{-2}) > Fe_3O_4/GC (0.0308 cm^{-2}).Therefore, after GCE was modified with Fe_3O_4/r-GO, the electroactive surface area increased relative to that modified with r-GO, indicating that the introduction of the magnetic grapheme nanohybrid provide more conduction pathways for the electron-transfer of $Fe(CN)_6^{3-/4-}$. In addition, the electrode modified with Fe_3O_4 nanoparticles possesses the least electroactive surface area between the above electrodes which is mostly attributed to the repulsion between $Fe(CN)_6^{3-/4-}$ probe molecule and negative surface charges of nanoparticles as well as relatively agglomerated nature of nanoparticles themselves. However, integrating them with grapheme nanosheets leads to greatly increase the electrochemical activity, indicating that grapheme nanosheets play an important role in enhancing Fe_3O_4 activity. Electrochemical impedance spectroscopy (EIS) is also an efficient tool for studying the interface properties of surface-modified electrodes. Thus, the electron transfer capability of these different electrodes was investigated by electrochemical impedance technique (Fig. 1E). After fitting the data, the values of charge-transfer resistance (R_{ct}) for different electrodes were obtained in the following order: Fe_3O_4/GC (336.0 Ω) > GC(126.1 Ω) > r-GO/GC (54.9 Ω) > Fe_3O_4/r-GO/GC (37.6 Ω). Based on these results, it may be speculated that the best electrochemical behavior among the studied electrodes should be observed at Fe_3O_4/r-GO/GC electrode. The inset of Fig. 1E shows the electrochemical impedance spectrum of LDH/Fe_3O_4/r-GO/GC electrode.It can be seen that for LDH/Fe_3O_4/r-GO/GC, the value of R_{ct} (4900.0 Ω) significantly increases compared to the GC, suggesting that LDH enzyme was successfully immobilized onto the electrode surface.

The electrochemical redox behavior of the Fe_3O_4/r-GO/GC electrode was further studied by cyclic voltammetry. The cyclic voltammograms of this modified electrode in a deaerated PBS (pH 7.0) at various potential scan rates were recorded (Fig. S1). As can be seen, there exist an anodic peak of ca. 0.0 V as well as a cathodic peak of ca.-0.15 V. The peak potentials separation (ΔE_p) is about 120 mV and the ratio of cathodic to anodic peak current i_{pc}/i_{pa} nearly equals to unity. The observed electrochemical behavior for Fe_3O_4/r-GO modified electrode could be attributed to the iron phosphate redox system. At first, Fe_3O_4 nanoparticles directly reduced at the electrode surface according to the following reaction:

$$Fe_3O_4(s)+2e^-+6H^+(aq)\rightarrow 2Fe^{2+}(aq)+3H_2O+FeO(s) \quad (1)$$

Then, Fe^{2+} ions produced could combine with phosphate ions in the buffer solution:

$$Fe^{2+}(aq)+HPO_4^{2-}(aq)\rightarrow FePO_4(s)+e^-+H^+(aq) \quad (2)$$

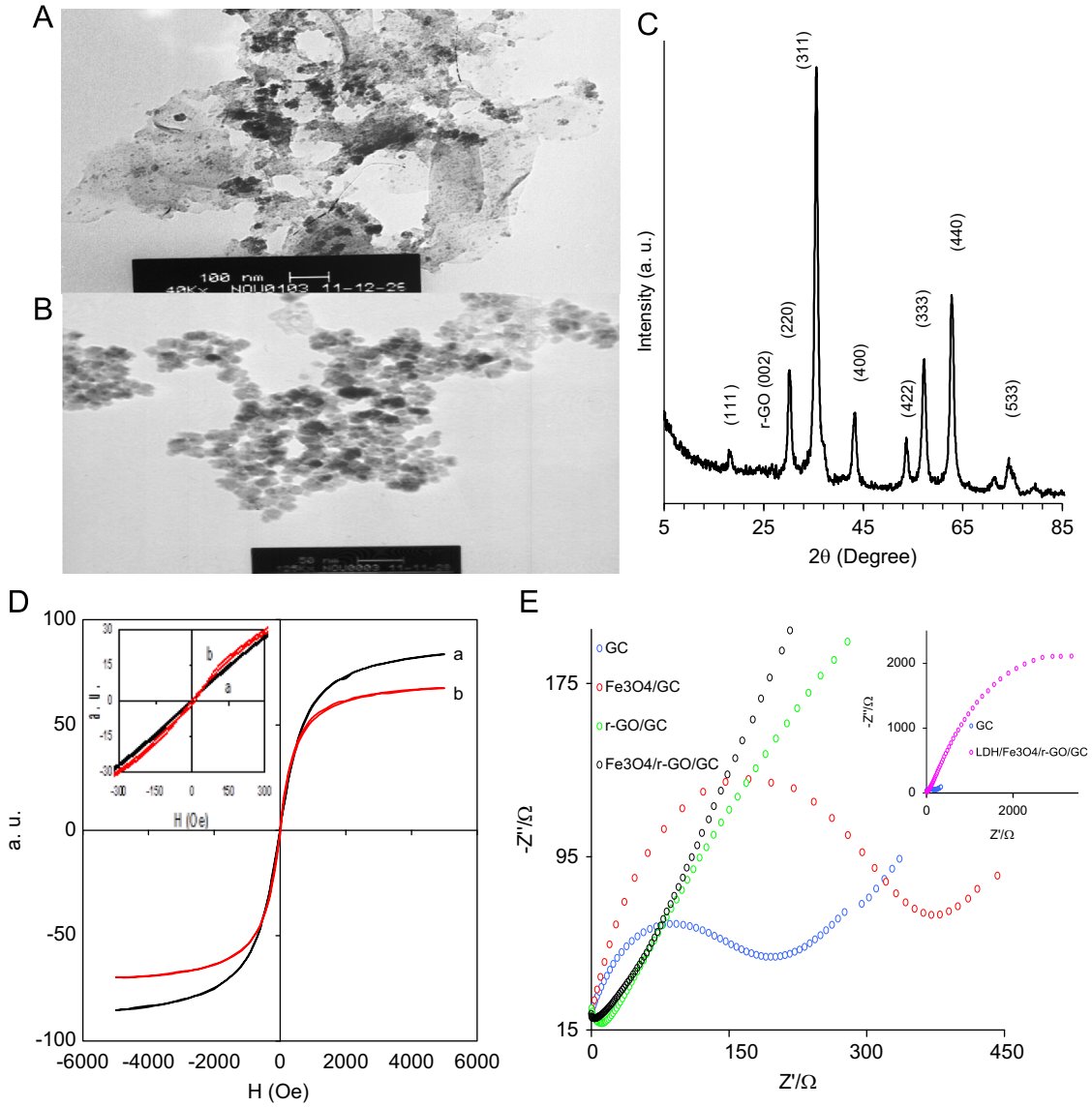

Fig. 1. (A) Low and (B) high magnification TEM images of Fe_3O_4/r-GO nanocomposite. (C) XRD pattern of Fe_3O_4/r-GO nanocomposites. (D) Room temperature magnetization curves of (a) Fe_3O_4 nanoparticles and (b) Fe_3O_4/r-GO nanocomposites. (E) EIS plots of 1.0 mM $[Fe(CN)_6]^{3-/4-}$ in 0.1 M KCl recorded at different electrodes of GC, Fe_3O_4/GC, r-GO/GC and Fe_3O_4/r-GO/GC. The inset of Fig. 1E shows the EIS plots of LDH/Fe3O4/r-GO/GC and GC electrodes.

Here after, the solid $FePO_4$ at the surface of electrode could be responsible for observed redox behavior (McKenzie and Marken, 2001; Teymourian et al., 2012).The plot of anodic and cathodic peak currents vs. scan ratewas recorded (inset A of Fig. S1). As can be seen, the peak currents were directly proportional to the scan rate in the whole rangestudied supported the idea of a surface-confined redox process. Moreover, the plotted E_p vs. log of scan rate (inset B of Fig. S1) shows that at high sweep rates, peak separations begin to increase indicating limitation due to the charge transfer kinetics. Based on the Laviron theory (Laviron, 1979), the heterogeneous electron transfer rate constant (k_s) and charge transfer coefficient (α) were obtained as 31.62 s^{-1} and 0.26, respectively. The large value of k_s indicates high ability of r-GO as an electron carrier for promoting electron transfer between Fe_3O_4 nanoparticles and electrode surface.

3.3. *Electrocatalysis of O_2 and H_2O_2 at the Fe_3O_4/r-GO/GC electrode*

At first, H_2O_2 and oxygen were selected to study the electrocatalytic behavior of Fe_3O_4/r-GO nanocomposite. Fig. 2(A and B) compares the cyclic voltammograms (CVs) for different electrodes of Fe_3O_4/GC, r-GO/GC and Fe_3O_4/r-GO/GC in the absence and presence of O_2 and H_2O_2. An obvious reduction wave of O_2 at the Fe_3O_4/r-GO/GC could be observed at −0.3 V with onset potential of 0.0 V that was more positive than ones obtained for Fe_3O_4/GC and r-GO/GC electrodes (Fig. 2A). Furthermore, according to the Fig. 2B, while both Fe_3O_4/GC and r-GO/GC electrodes hardly responded for such concentration of H_2O_2, the electrode loaded with Fe_3O_4/r-GO nanocomposite exhibited significantly enhanced currents for both the oxidation and reduction of H_2O_2 starting around +0.45 V and +0.05 V, respectively. It was believed that while the Fe_3O_4 nanoparticles are mainly responsible for observed electrocatalytic behavior at Fe_3O_4/r-GO nanocomposite modified electrode, however, the existence of graphene nanosheets as a carbon support with excellent electronic conduction features is essential to the dispersion of these nanoparticles so as to fully utilize their catalytic properties and in fact, the superior electrocatalytic activity of the Fe_3O_4/r-GO film modified electrode can be attributed to the good synergistic coupling effects between the Fe_3O_4 nanoparticles and r-GO nanosheets. Thus, the Fe_3O_4/r-GO modified electrode not only improves the redox currents but also decreases the overvoltage potential for the O_2 reduction as well as

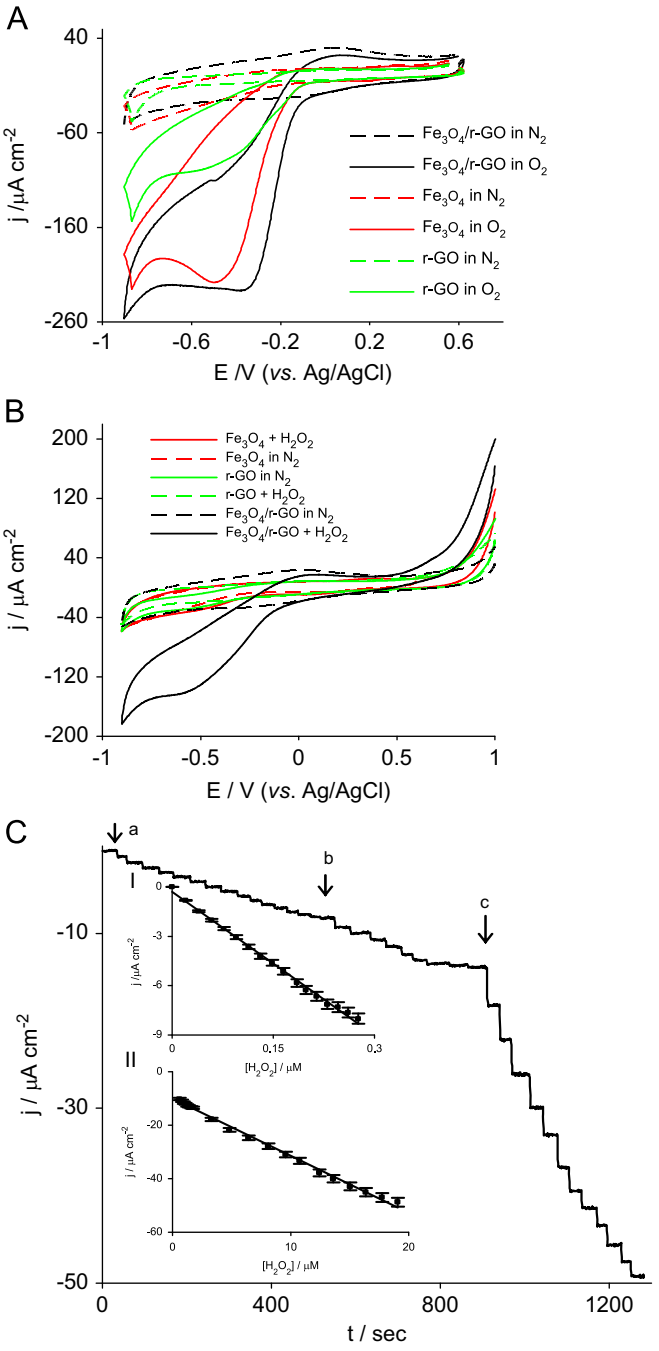

Fig. 2. (A) CVs of Fe_3O_4/GC, r-GO/GC and Fe_3O_4/r-GO/GC electrodes in 0.1 M PBS at pH 7.0 at various conditions (scan rate 0.02 V s^{-1}). (B) CVs of Fe_3O_4/GC, r-GO/GC and Fe_3O_4/r-GO/GC electrodes in deaerated 0.1 M PBS at pH 7.0 in the absence and presence of 0.4 mM H_2O_2. (C) Current–time curve for Fe_3O_4/r-GO/GC electrode with successive H_2O_2 additions of 0.02 μM (a), 0.2 μM (b) and 2 μM (c). Electrolyte: 0.1 M PBS (pH 7.0). Applied potential: −0.3 V. (Insets I and II are the correspondent calibration curves for lower and higher concentration ranges, respectively).

for the oxidation and reduction of H_2O_2, allowing convenient low-potential amperometric detection. The amperometric responses of the Fe_3O_4/r-GO/GC electrode to the successive additions of different concentrations of H_2O_2 at applied potential of −0.3 V along with the resulting calibration plot are given in Fig. 2(C). As can be seen from this amperogram, well-defined and fast amperometric signals are observed from H_2O_2 additions, generating steady-state signals within 1–2 s. Referring Table 1A that summarizes the response characteristics of the Fe_3O_4/r-GO/GC electrode obtained for different analytes, the linear range for H_2O_2 is 0.02–19 μM at the proposed nanocomposite modified electrode. Also the detection limit of H_2O_2 was calculated as 6 nM ($S/N=3$). This result is lower than those at other H_2O_2 sensors, such as CNTs/chitosan modified electrode (10.3 μM at −0.2 V) (Qian and Yang, 2006), reduced graphene oxide/ferro-ferric nanocomposite modified electrode (3.2 μM at -0.3 V) (Ye et al., 2012), chemically reduced graphene oxide/Ag nanoparticles modified electrode (31.3 μM at −0.3 V) (Liu et al., 2011), Au/graphene/HRP/chitosan modified electrode (1.7 μM at −0.3 V) (Zhou et al., 2010), graphene/Au NPs/chitosan (180 μM at −0.2 V) (Shan et al., 2010) and silver nanoparticles capped in a PVA film modified Pt electrode (1.0 μM at −0.5 V) (Guascitoa et al., 2008), indicating that Fe_3O_4/r-GO can serve as an excellent choice for the enhanced electrochemical sensing. Additionally, very good reproducibility was obtained using the same Fe_3O_4/r-GO/GC electrode for 10 repetitive amperometric analyses of 1.0 μM H_2O_2 at applied potential of −0.3 V resulting in a relative standard deviation of 3.8%. In order to study the reproducibility of the electrode modification, five modified electrodes were prepared independently. The RSD for determining 10 μM H_2O_2 was 6.3%. The Fe_3O_4/r-GO-based H_2O_2 sensor also exhibited a good long-termstability. The catalytic current response can maintain about 95% of its initial value even after one month.

3.4. Electrocatalytic oxidation of NADH and lactate biosensing

The electrochemical oxidation of NADH to the corresponding oxidized form (NAD^+) in aqueous solution has received considerable interest, owing to its significance both as a substrate for dehydrogenase enzymes and also to the design of the novel biosensors, because NAD^+/NADH-dependent dehydrogenases constitute the largest group of redox enzymes known today (Bartlett et al., 2002). In Fig. 3A, CVs for NADH oxidation at different electrodes were compared. As can be seen, in the case of the Fe_3O_4/r-GO/GC electrode, the anodic potential of NADH shifted negatively to 0.0 V and exhibited highly increased current signal in comparison with r-GO/GC and Fe_3O_4/GC electrodes. Here, the excellent electrochemical behavior of Fe_3O_4/r-GO nanocomposite-based system toward electrooxidation of NADH may be attributed to the promising mediator-like electrocatalytic activity of Fe_3O_4 NPs as well as high electron transfer kinetics on grapheme nanosheets. In this system, Fe_3O_4 plays the role of an electrocatalyst for NADH oxidation while r-GO acts as an electron carrier. The mechanism of the electrochemical NADH oxidation in

Table 1A
Response characteristics of different analytes on Fe_3O_4/r-GO nanocomposite modified electrode.

Analyte	Applied potential (V)	Linear range (M)	Detection limit (M)	Sensitivity (A M^{-1} cm^{-2})
H_2O_2	−0.3	2×10^{-8}–2.8×10^{-7}	6×10^{-9}	29.18
NADH	+0.05	2.8×10^{-7}–1.9×10^{-5} 2×10^{-6}–1.5×10^{-5}	– 4×10^{-7}	2.262 0.113
Lactate	+0.1[a]	1.5×10^{-5}–1.9×10^{-4} 2×10^{-4}–2.2×10^{-3}	– 2×10^{-5}	0.034 0.0226
AA	+0.01[a]	1.6×10^{-4}–7.2×10^{-3}	2×10^{-5}	0.0335
DA	+0.16[a]	4×10^{-7}–3.5×10^{-6}	8×10^{-8}	38.8
UA	+0.33[a]	3.5×10^{-6}–1.6×10^{-5} 4×10^{-6}–2×10^{-5}	– 5×10^{-7}	12.9 4.50
Nitrite	+0.7 −0.3	2×10^{-5}–2.1×10^{-4} 1×10^{-6}–9.2×10^{-5} 1×10^{-5}–1.6×10^{-4}	– 3×10^{-7} 1.2×10^{-6}	1.22 0.226 0.158

[a] The potential at which the electrocatalytic current was reported.

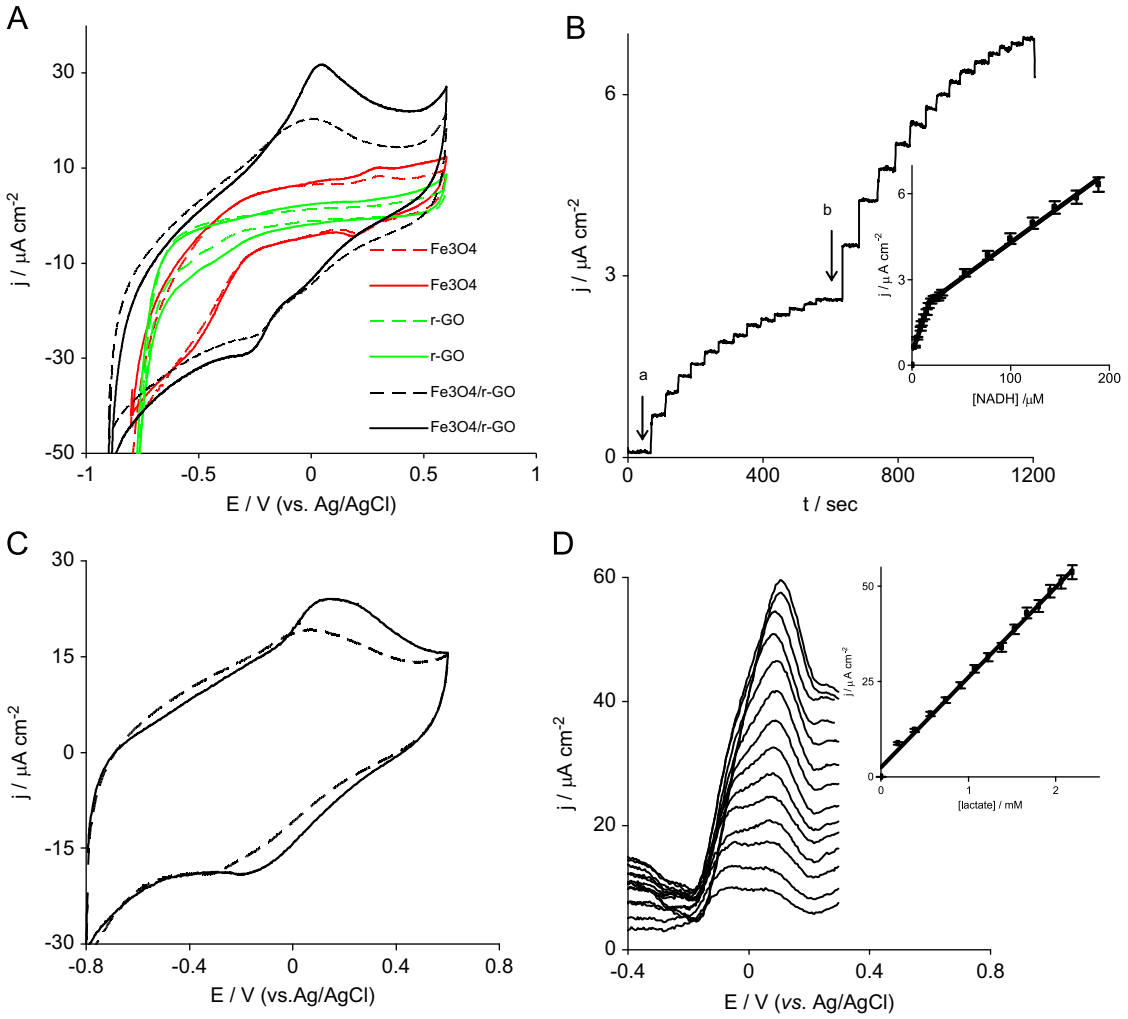

Fig. 3. (A) CVs of Fe_3O_4/GC, r-GO/GC and Fe_3O_4/r-GO/GC electrodes in 0.1 M PBS (pH 7.0) and scan rate 20 mV s^{-1} in the absence (dashed line) and presence (solid line) of 0.5 mM NADH. (B) Chronoamperometric response of Fe_3O_4/r-GO/GC electrode in PBS (0.1 M, pH 7.0) on successive addition of different NADH concentrations of 2.5 μM (a) and 25 μM(b) at working potential of 0.1 V vs. Ag/AgCl. Inset is the plot of amperometric response vs. NADH concentration. (C) CVs of LDH/Fe_3O_4/r-GO/GC electrode in 0.1 M PBS (pH 7.0) containing 5 mM NAD^+ and scan rate 20 mV s^{-1} in the absence (dashed line) and presence (solid line) of 1.0 mM lactate. (D) DPVs of LDH/Fe_3O_4/r-GO/GC electrode in 0.1 M PBS (pH 7.0) containing 5 mM NAD^+at different lactate concentrations, (from inner to outer) 0.2, 0.38, 0.57, 0.74, 0.91, 1.07, 1.23, 1.38, 1.52, 1.67, 1.8, 1.93, 2.06 and 2.19 mM.Inset is the plot of peak currents vs. lactate concentration (data obtained were the averages of three measurements).

the suggested system is as follows:

$$Fe_3O_4/r-GO + NADH \underset{K_{-1}}{\overset{K_1}{\rightleftarrows}} Fe_3O_4/r-GONADH \xrightarrow{K_2} Fe_3O_4/r–GO + NAD^+ \quad (3)$$

$$Fe_3O_4/r\text{-}GONADH \rightarrow Fe_3O_4/r\text{-}GONADH^{+}+e^- \quad (4)$$

$$Fe_3O_4/r\text{-}GONADH^{\bullet+} \rightarrow Fe_3O_4/r\text{-}GONAD+H^+ \quad (5)$$

$$Fe_3O_4/r\text{-}GONAD^{\bullet} \rightarrow Fe_3O_4/r\text{-}GONAD^{+}+e^- \quad (6)$$

where NADH diffuses and adsorbs on the electrode surface and then it is electrochemically oxidized by an ECE mechanism (Eq. (3)) (Moiroux and Elving, 1980). According to the ECE mechanism, the first step of NADH electrochemical oxidation is an irreversible heterogeneous electron transfer. In this step, one electron is lost and a cation radical $NADH^{\bullet+}$ is produced (Eq. (4)). The neutral radical $NAD^{\bullet}$ was produced through a first-order deprotonation reaction of $NADH^{\bullet+}$ (Eq. (5)). A continual reaction for electron transfer from $NAD^{\bullet}$ occurred through a second heterogeneous electron transfer (Eq. (6)).

Fig. 3B presents the amperometric response of the Fe_3O_4/r-GO/GC electrode at +0.05 V to the successive additions of NADH. Immediately after the addition of NADH, the anodic current increased and reached a steady state within <5 s. The sensor response displayed two linear concentration ranges (as in Table 1A); one from 2 to 15 μM ($R^2=0.994$) with sensitivity of 0.113 A $M^{-1}cm^{-2}$and another one from 15 to 190 μM ($R^2=0.996$) with a sensitivity of 0.034 A $M^{-1}cm^{-2}$. The limit of detection of this sensing system was determined as 0.40 μM ($S/N=3$). The analytical parameters for NADH detection at the proposed Fe_3O_4/r-GO nanocomposite modified electrode are comparable to other previously reported results (Huang et al., 2007; Yang and Liu, 2009; Kim et al., 2010). The kinetic parameters of this reaction can be estimated by plotting the NADH concentration vs. the current difference (inset of Fig. 3B). This plot showed the kinetics of a heterogeneous second-order reaction type, hence, the affinity of NADH for the electrode ($k_{-1}+k_2/k_1$ in Eq. (3)) can be estimated by a Michaelis–Menten constant (K_M) calculation; the value was 52.8 μM, deduced from a Lineweaver–Burk plot. The obtained K_M is lower compared to our previously reported value of 95 μM (Teymourian et al., 2012), that obviously implies the higher affinity of Fe_3O_4/r-GO/GC electrode toward NADH when compared to Fe_3O_4/MWCNT/GC electrode. Also this value is lower than other reported ones such as 3.04 mM (Kim et al., 2010), 0.54 mM (Kim and Yoo, 2009), 0.212 mM (Santos Alvarez et al., 2005) and 0.8 mM (Gligor et al., 2009). Moreover, the reproducibility of the Fe_3O_4/r-GO/GC electrode for NADH detection was examined. The chronoamperometric signals produced by a series of five successive measurements of 10 and

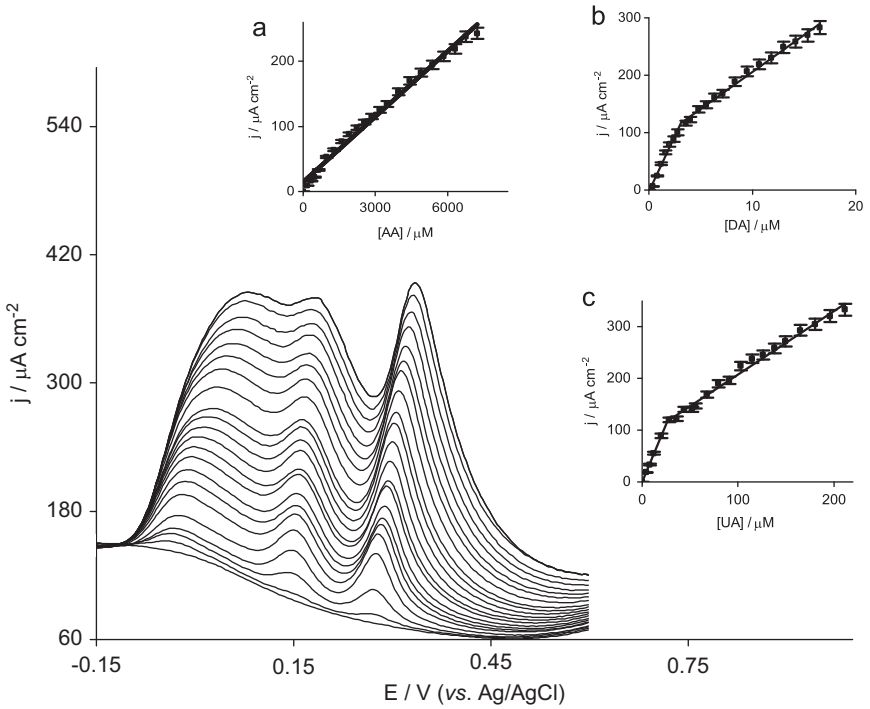

Fig. 4. DPVs of Fe_3O_4/r-GO/GC electrode in PBS (0.1 M, pH 7.0) containing mixed concentrations of the AA, DA and UA mixture. [AA]: 0.0, 0.3, 0.48, 0.64,0.96, 1.28, 1.59, 1.91, 2.23, 2.54, 2.86, 3.17, 3.49, 3.96, 4.43, 4.90, 5.37, 5.83, 6.30, 6.76 and 7.22 mM.[DA]: 0.0, 0.4, 0.8, 1.2, 1.6, 2.0, 2.39, 2.79, 3.59, 3.98, 4.78, 5.57, 6.36, 7.15, 8.33, 9.51, 10.68, 11.86, 13.03, 14.2, 15.36 and 16.52.[UA]: 0.0, 4.0, 8.0, 11.98, 19.96, 27.92, 35.87, 43.81, 51.73, 55.69, 67.54, 79.36, 91.16, 102.93, 114.67, 126.38, 138.07, 149.72, 165.22, 180.68, 196.08, 211.43. Insets are the plots of oxidation peak currents vs. AA (a), DA (b) and UA (c) concentrations.

100 μM NADH yielded good reproducibilities with the relative standard deviations of 4.8 and 5.2%, respectively.

Using LDH as the model biorecognition element, we further demonstrated the use of the LDH/Fe_3O_4/r-GO nanobiocomposite as an electronic transducer for the development of an electrochemical biosensor for lactate. Fig. 3C shows the CVs of LDH/Fe_3O_4/r-GO/GC electrode containing 5 mM NAD^+ cofactor in the absence and presence of 1.0 mM lactate. As indicated, the anodic peak current increased in the presence of lactate with the onset potential of 0.0 V reaching the maximum current at 0.15 V. DPVs of LDH/Fe_3O_4/r-GO/GC electrode for successive additions of lactate were recorded (Fig. 3D). This observation clearly supports that the increasing in peak observed at +0.1 V is due to the oxidation of enzymatically produced NADH during lactate oxidation. The calibration plot drawn between the response current and the concentration of lactate (0.2–2.2 mM) is found to be linear with sensitivity of 0.0226 A $M^{-1}cm^{-2}$, and the detection limit was calculated as 20 μM (Table 1A). The data obtained here further confirm the efficiency of Fe_3O_4/r-GO nanocomposite both as a mediatorless electrocatalyzing material and also as an excellent platform for immobilization of enzymes and construction of biosensing devices.

3.5. Electrochemical detection of AA, DA and UA at Fe_3O_4/r-GO/GC electrode

Ascorbic acid (AA), dopamine (DA), and uric acid (UA) are electroactive compounds that have similar electrochemical properties, which complicate their electrochemical identification (Sun et al., 2011). Fig. 4 depicts the DPV recordings at various concentrations of AA, DA and UA at Fe_3O_4/r-GO/GC electrode. As can be seen, three well-defined separated anodic peaks corresponding to oxidation of AA, DA and UA are observed at potentials of approximately 0.01, 0.16 and 0.33 V, respectively. The oxidation peak current of these three molecules linearly increases with their concentrations. For AA (Fig. 4A), the linear egression equation is calibrated as j_{AA} (μA cm^{-2})= 14.833+0.0335[AA] (μM) ([AA]:160.0–7227.1 μM, R^2=0.9993). For DA (Fig. 4B), two linear regression equations were obtained which are expressed as j_{DA} (μA cm^{-2})= −2.8705+38.771[DA] (μM) ([DA]:0.4–3.5 μM, R^2=0.9992) and j_{DA} (μA cm^{-2})= 77.213+12.844 [DA] (μM) ([DA]:3.5–160.0 μM, R^2=0.9995). In the case of UA (Fig. 4C), two linear regression equations were also obtained which are calculated as j_{UA} (μA cm^{-2})= −0.1579+4.474 [UA] (μM) ([UA]:4.0–20.0 μM, R^2=0.9998) and j_{UA} (μA cm^{-2})= 86.052+1.224 [UA] (μM) ([UA]:20.0–212.0 μM, R^2= 0.9996). The detection limits (S/N=3) for the determination of AA, DA and UA were evaluated as 20.0 μM, 0.08 μM and 0.50 μM, respectively (Table 1A). The lowest detection limits obtained here for simultaneous determination of AA, DA and UA are comparable or in some cases better than previously reported values such as 50, 0.02 and 0.2 μM at mesoporous carbon nanofiber modified pyrolytic graphite electrode (Yue et al., 2012), 20, 0.5 and 0.4 μM at ordered mesoporous carbon/nafion composite film (Zheng et al., 2009) and 3, 0.09 and 0.3 μM at iron(III)–porphyrine functionalized MWCNTs (Wang et al., 2012).

3.6. Electrocatalytic determination of nitrite at Fe_3O_4/r-GO/GC electrode

In order to further demonstrate the usefulness of the proposed Fe_3O_4/r-GO nanocomposite-based platform, its ability toward sensing nitrite as an important inorganic analyte has been surveyed. Fig. 5A presents the CVs for Fe_3O_4/r-GO/GC electrode in the absence and presence of different concentrations of nitrite. As can be seen, the Fe_3O_4/r-GO nanocomposite exhibited significantly enhanced currents for both the oxidation and reduction of nitrite starting around +0.5 V and +0.3 V, respectively. Such a high electrocatalytic behavior of the Fe_3O_4/r-GO modified electrode for the oxidation and reduction of nitrite can be exploited to

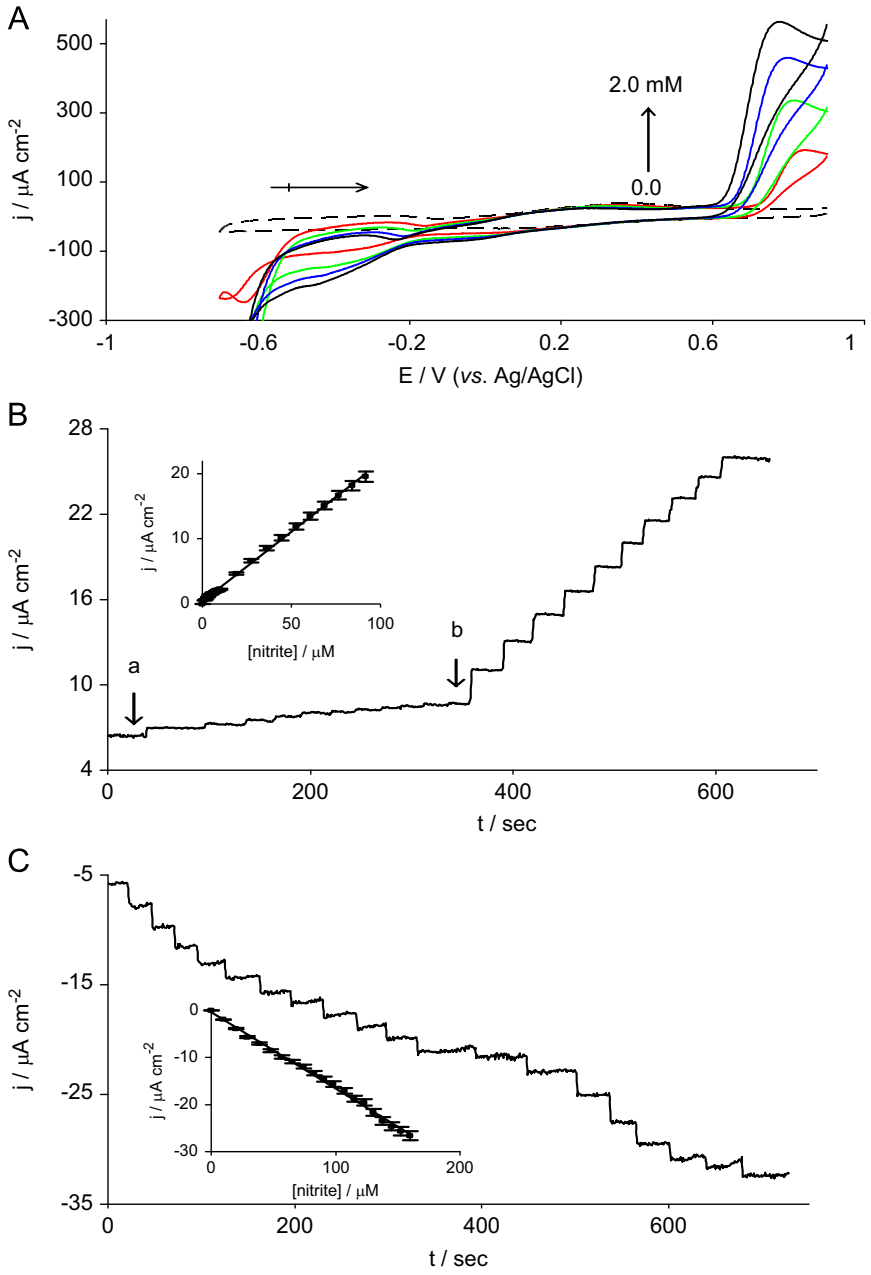

Fig. 5. (A) CVs of Fe_3O_4/r-GO/GC electrode in 0.1 PBS pH 2.0 at scan rate 20 mV s^{-1} with increasing nitrite concentration of 0.0, 0.5, 1.0, 1.5 and 2.0 mM.(B, C) Current–time responses at Fe_3O_4/r-GO/GC electrode in 0.1 PBS with successive additions of 1.0 (a) and 10.0 μM (b) in B and 10.0 μM in C (Applied potentials: +0.7 V in B and −0.4 V in C). Insets show the relationship between oxidation and reduction currents with the concentration of nitrite.

convenient low-potential amperometric detection of nitrite. The amperometric responses of the Fe_3O_4/r-GO/GC electrode to the successive additions of different concentrations of nitrite at applied potentials of +0.7 V and -0.4 V along with the resulting calibration plots are given in Fig. 5 (B and C), respectively. As can be seen from these amperograms, well-defined and fast amperometric signals are observed from nitrite additions, generating steady-state signals within less than 3 s. The linear ranges for nitrite (Table 1A) were obtained as 1–92 μM and 10–160 μM based on its oxidation and reduction at the proposed nanocomposite modified electrode, respectively. Also the detection limits of nitrite at the Fe_3O_4/r-GO/GC electrode were calculated as 0.3 μM (at +0.7 V, based on $S/N=3$) and 1.2 μM (at −0.3 V, based on $S/N=3$).The analytical performances obtained above are comparable to or better than those of the other nitrite sensors (Dreyse et al., 2011; Mani et al., 2012).

Table 1B
Determination of nitrite in sausage samples by using Fe_3O_4/r-GO nanocomposite modified electrode.

Sample no.	Amount found[a] (ppm)		Added (ppm)	Found (ppm)	Recovery (%)
	Griess method	Proposed sensor			
1	71.09 ± 2.06	72.85 ± 3.69	8	83.37	103.12
2	95.33 ± 1.64	98.19 ± 3.20	8	108.91	102.56

[a] Mean value for triplicate measurments.

In order to further demonstrate the good performance of the proposed sensing system, its applicability was evaluated by the analysis of nitrite as a model analyte in real samples. The obtained results were given in Table 1B. It could be seen that there is a good

agreement between the values obtained by our proposed methodology and the spectroscopic reference method and also between the spiked and found values for detection of nitrite. These results clearly indicate that the system presented here to be valid for the real samples analysis.

4. Conclusion

In this paper, a facile one-step synthetic route (a chemical reaction strategy including the reduction of GO and the in-situ generation of Fe_3O_4 nanoparticles)was used to produce Fe_3O_4/r-GO nanocomposite. The new nanohybrid material combines the unique and attractive electronic behavior of r-GO nanosheets with excellent catalytic properties of Fe_3O_4 nanoparticles. The resulting nanocomposite was investigated by various characterization methods, including TEM, XRD, AGFM and EIS. Fe_3O_4/r-GO nanocomposite modified GC electrode was reported as a novel electrode system for the preparation of electrochemical sensing and biosensing platform and the electrocatalytic behaviors of different kinds of important electroactive compounds (H_2O_2, NADH, nitrite, neurotransmitters (dopamine (DA)), and other biomolecules (ascorbic acid (AA) and uric acid (UA)) at the Fe_3O_4/r-GO/GC electrode were assessed. Electrochemical studies verified that the Fe_3O_4/r-GO/GC electrode possess excellent electrocatalytic activities toward all these analytes because of the synergistic integration of the two nanomaterials. As demonstrated here, r-GO sheets are uniquely advantageous to serve as a conductive support to uniformly anchor Fe_3O_4 magnetic nanoparticles with well-defined size and shapes. Agglomeration, the common phenomenon of metallic oxide preparations, is no longer an issue. Above all, the Fe_3O_4/r-GO hybrid could be an extremely promising candidate applicable for a wide range of electrochemical sensing and biosensing applications.

Acknowledgments

The financial support of University of Kurdistan is gratefully acknowledged. Hazhir Teymourian also thanks the Iranian Nanotechnology Initiative for Postdoc fellowship.

Appendix A. Supporting information

Supplementary data associated with this article can be found in the online version at http://dx.doi.org/10.1016/j.bios.2013.04.034.

References

Bartlett, P.N., Simon, E., Toh, C.S., 2002. Bioelectrochemistry 56, 117–122.
Chandra, V., Park, J.S., Chun, Y., Lee, J.W., Hwang, I.C., Kim, K.S., 2010. ACS Nano 4, 3979–3986.
Cong, H.P., He, J.J., Lu, Y., Yu, S.H., 2010. Small 6, 169–173.
Dreyse, P., Isaacs, M., Calfumán, K., Cáceres, C., Aliaga, A., Aguirre, M.J., Villagra, D., 2011. Electrochimica Acta 56, 5230–5237.
Gligor, D., Dilgin, Y., Popescu, I.C., Gorton, L., 2009. Electrochimica Acta 54, 3124–3128.
Guascitoa, M.R., Filippo, E., Malitesta, C., Manno, D., Serra, A., Turco, A., 2008. Biosensors and Bioelectronics 24, 1057–1063.
He, F., Fan, J.T., Ma, D., Zhang, L.M., Leung, C., Chan, H.L., 2010. Carbon 48, 3139–3144.
He, H.K., Gao, C., 2010. ACS Applied Materials and Interfaces 2, 3201–3210.
He, Y., Sheng, Q., Zheng, J.B., Wang, M.Z., Liu, B., 2011. Electrochimica Acta 56, 2471–2476.
Huang, M., Jiang, H., Zhai, J., Liu, B., Dong, S., 2007. Talanta 74, 132–139.
Hummers, W.S., Offeman, R.E., 1958. Journal of the American Chemical Society 80, 1339 1339.
Kim, Y.H., Yoo, Y.J., 2009. Enzyme and Microbial Technology 44, 129–134.
Kim, Y.H., Kim, T., Ryo, J.H., Yoo, Y.J., 2010. Biosensors and Bioelectronics 25, 1160–1165.
Laviron, E., 1979. Journal of Electroanalytical Chemistry 101, 19–28.
Li, D., Muller, M.B., Gilje, S., Kaner, R.B., Wallace, G.G., 2008. Nature Nanotechnology 3, 101–105.
Liu, S., Tian, J., Wang, L., Sun, X., 2011. Carbon 49, 3158–3164.
Mani, V., Periasamy, A.P., Chen, S.M., 2012. Electrochemistry Communications 17, 75–78.
Massart, R., 1981. IEEE Transactions on Magnetics 17, 1247–1248.
McKenzie, K.J., Marken, F., 2001. Pure and Applied Chemistry 73, 1885–1894.
Moiroux, J., Elving, P.J., 1980. Journal of the American Chemical Society 102 (21), 6533–6538.
Navaee, A., Salimi, A., Teymourian, H., 2012. Biosensors and Bioelectronics 31, 205–211.
Pumera, M., 2009. Chemical Record 9, 211–223.
Qian, L., Yang, X., 2006. Talanta 68, 721–727.
Santos Alvarez, D.N., Castanon, M.J.L., Ordieres, A.J.M., Blanco, P.T., Abruna, H.D., 2005. Analytical Chemistry 77, 2624–2631.
Shan, C., Yang, H., Han, D., Zhang, Q., Ivaska, A., Niu, L., 2010. Biosensors and Bioelectronics 25, 1070–1074.
Si, Y.C., Samulski, E.T., 2008. Chemistry Materials 20, 6792–6797.
Su, J., Cao, M.H., Ren, L., Hu, C., 2011. The Journal of Physical Chemistry C115, 14469–14477.
Sun, C.L., Lee, H.H., Yang, J.M., Wu, C.C., 2011. Biosensors and Bioelectronics 26, 3450–3455.
Tang, D., Tang, J., Li, Q., Liu, B., Yang, H., Chen, G., 2011. RSC Advances 1, 40–43.
Teymourian, H., Salimi, A., Hallaj, R., 2012. Biosensors and Bioelectronics 33, 60–68.
Wang, C., Yuan, R., Chai, Y., Chen, S., Zhang, Y., Hu, F., Zhang, M., 2012. ElectrochimicaActa 62, 109–115.
Wang, G., Shen, X., Wang, B., Yao, J., Park, J., 2009. Carbon 47, 1359–1364.
Wang, X., Zhi, L.J., Mullen, K., 2008. Nano Letters 8, 323–327.
Yang, D.W., Liu, H.H., 2009. Biosensors and Bioelectronics 25, 733–738.
Ye, Y., Kong, T., Yu, X.F., Wu, Y., Zhang, K., Wang, X.P., 2012. Talanta 89, 417–421.
Yue, Y., Hu, G., Zheng, M., Guo, Y., Cao, J., Shao, S., 2012. Carbon 50, 107–114.
Zheng, D., Ye, J., Zhou, L., Zhang, Y., Yu, C., 2009. Journal of Electroanalytical Chemistry 625, 82–87.
Zhou, K., Zhu, Y., Yang, X.L., Luo, J., Li, C.Z., Luan, S.R., 2010. Electrochimica Acta 55, 3055–3060.
Zhou, M., Zhai, Y., Dong, S., 2009. Analytical Chemistry 81, 5603–5613.
Zhu, Y., Stoller, M.I.D., Cai, W., Velamakanni, A., Piner, R.D., Chen, D., Ruoff, R.S., 2010. ACS Nano 4, 1227–1233.